

Nonlinear resonance and devil's staircase in a forced planer system containing a piecewise linear hysteresis

Yuu Miino

*Advanced Tech. and Science, System Innovation Engineering, Tokushima University,
2-1 Minami-Josanjima-Cho, Tokushima 770-8506, Japan
c501647001@tokushima-u.ac.jp*

Tetsushi Ueta

*Center for Admin. Info. Tech. Tokushima University,
2-1 Minami-Josanjima-Cho, Tokushima 770-8506, Japan
ueta@tokushima-u.ac.jp*

Hiroshi Kawakami

*Professor emeritus of Tokushima University,
2-1, Minami-Josanjima-Cho, Tokushima 770-8506, Japan
h.kawakami@384.jp*

Abstract

The Duffing equation describes a periodically forced oscillator model with a nonlinear elasticity. In its circuitry, a saturable-iron core often exhibits a hysteresis, however, a few studies about the Duffing equation has discussed the effects of the hysteresis because of difficulties in their mathematical treatment. In this paper, we investigate a forced planer system obtained by replacing a cubic term in the Duffing equation with a hysteresis function. For simplicity, we approximate the hysteresis to a piecewise linear function. Since the solutions are expressed by combinations of some dynamical systems and switching conditions, a finite-state machine is derived from the hybrid system approach, and then bifurcation theory can be applied to it. We topologically classify periodic solutions and compute local and grazing bifurcation sets accurately. In comparison with the Duffing equation, we discuss the effects caused by the hysteresis, such as the devil's staircase in resonant solutions.

Keywords: bifurcation analysis, hybrid system, nonlinear resonance, Duffing equation, devil's staircase, chaos

1. Introduction

The Duffing equation describes a typical nonlinear non-autonomous system that provides a rich variety of nonlinear phenomena: a horseshoe structure around a saddle fixed point[1], nonlinear resonance with jump phenomena, bifurcations of periodic solutions, chaotic behavior[2] and so on. It has been already well studied from viewpoints varying from mathematical analyses[3] to control engineering[4].

The circuit corresponding to the Duffing equation is achieved by a resistor, a capacitor and a nonlinear inductor with an external driving force[3, 5], see Fig. 1. Conventionally, the current of the inductor is approximated by a third-power poly-

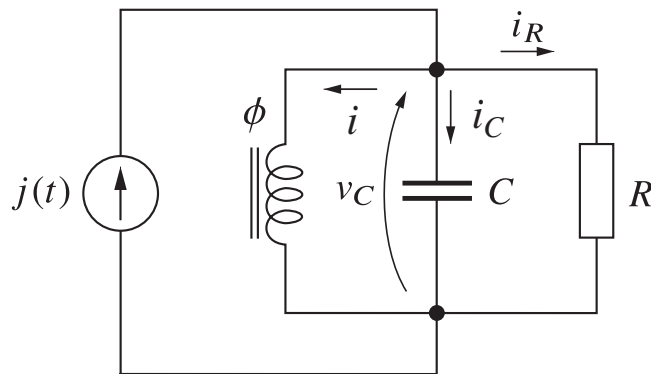


Figure 1: A forced resonant circuit with a saturable-core inductor.

mial of the magnetic flux. However, a practical saturable-core inductor has a hysteresis between the current and the flux. The Duffing equation containing the hysteresis was investigated, e.g., Hayashi[6] suggested that the hysteresis affects structures of bifurcation sets for periodic solutions.

To analyze a nonlinear system rigorously, piecewise linear (PWL) functions are frequently used to approximate these nonlinear characteristics and, conversely, sometimes utilized to create complex behavior[7]. For example, Nishio and Mori[8] showed chaotic phenomena derived from a two-dimensional circuit with a PWL hysteresis and Kimura *et al.*[9] presented an application of a PWL system. Kousaka *et al.*[10] developed a general method to solve bifurcation problems of nonlinear systems containing hysteresis.

Nonsmooth systems appear naturally in many practical systems because many physical phenomena present discontinuities: switching in an electrical circuit[11], firing in the neuronal systems[12] or having impacts in mechanics[13]. Their discontinuities can be approximated by the PWL functions.

In this study, we discuss the behavior observed in a forced planer system obtained by replacing a cubic term in the Duffing equation with a hysteresis function. We regard these properties as a simple PWL function in order to apply the hybrid system approaches. In Section 2, we introduce the Duffing equation with its circuitry. We also provide mathematical preliminaries for the hybrid system with hysteresis in this section. We try to describe the hysteresis by defining departure and arrival sets and determine the relationship among them. Then the system provides a finite-state machine (FSM), which is necessary for constructing the hybrid system. In Section 3, we briefly denote topological classifications of periodic solutions and their bifurcations. In Section 4, we show bifurcation diagrams and response curves of periodic solutions in the system by solving the fixed point equation and the characteristic equation simultaneously. We compare the bifurcation structures between the Duffing equation and the proposed hybrid system and point out their differences and similarities. We introduce the ratio ρ as a measure to represent a characteristic of the solutions of the proposed system and observe the devil's staircase in the ratio ρ , which cannot be found in the Duffing equation. Finally, we conclude this study in Section 5.

2. Duffing equation containing a piecewise linear hysteresis

2.1. Duffing equation

The resonant circuit shown in Fig. 1 leads to the following equations:

$$\begin{aligned}
 C \frac{dv_C}{dt} + \frac{v_C}{R} + i &= j(t), \\
 N \frac{d\phi}{dt} &= v_C, \\
 Ni &= G(\phi) = a_1\phi + a_3\phi^3, \\
 j(t) &= J_0 + J \cos \omega t,
 \end{aligned} \tag{1}$$

where ϕ is the magnetic flux of the saturable-core inductor, N is the number of turns of the coil, and G is the characteristic of the inductor that is assumed to be a cubic function. By taking variable transformations such as:

$$\begin{aligned} x &= \phi, \quad \tau = \omega t, \\ k &= \frac{1}{\omega RC}, \quad c_1 = \frac{a_1}{N^2 \omega^2 C}, \quad c_3 = \frac{a_3}{N^2 \omega^2 C}, \\ g(x) &= c_1 x + c_3 x^3, \quad B_0 = \frac{J_0}{N \omega^2 C}, \quad B = \frac{J}{N \omega^2 C}, \end{aligned}$$

we have

$$\frac{d^2 x}{d\tau^2} + k \frac{dx}{d\tau} + g(x) = B_0 + B \cos \tau. \quad (2)$$

By setting $dx/d\tau$ with y and rewriting τ as t , Eq. (2) can be written as a system of first-order ordinary differential equations on \mathbf{R}^2 :

$$\frac{dx}{dt} = y, \quad \frac{dy}{dt} = -ky - g(x) + B_0 + B \cos t. \quad (3)$$

We call Eq. (3) the Duffing equation[2]. Several variations of circuit implementation and equations for the Duffing equation have been revisited by Kovacic and Brennan [3].

2.2. Hysteresis of a saturable-core inductor and its piecewise linear approximation

A saturable-core inductor includes the hysteresis in the relationship between the magnetic flux ϕ and the current i of the inductor, as shown in Fig. 2 (a). In accordance with the magnetic saturation and the remanence of the iron core, a hysteresis loop is formed by varying the flux, i.e., if an increment of the flux exceeds a threshold ϕ_1 , a decrement may trace another curve (lower curve in the figure). Also after the negative threshold ϕ_{-1} in the decrement is exceeded, the flux may trace the other curve (upper curve in the figure) in the increment, where the thresholds ϕ_1 and ϕ_{-1} correspond remanences. The appearance of the gap between these curves is the main property of the hysteresis. The state of the saturable-core inductor, magnetized or not, determines which curve the current follows; and therefore, it actually includes a memory in a sense.

We try to approximate the hysteresis to a PWL hysteresis H constructed of two PWL functions shown in Fig. 2 (b)[8]. Note $x_{th}(\pm 1)$ is in accordance with $\phi_{\pm 1}$, and

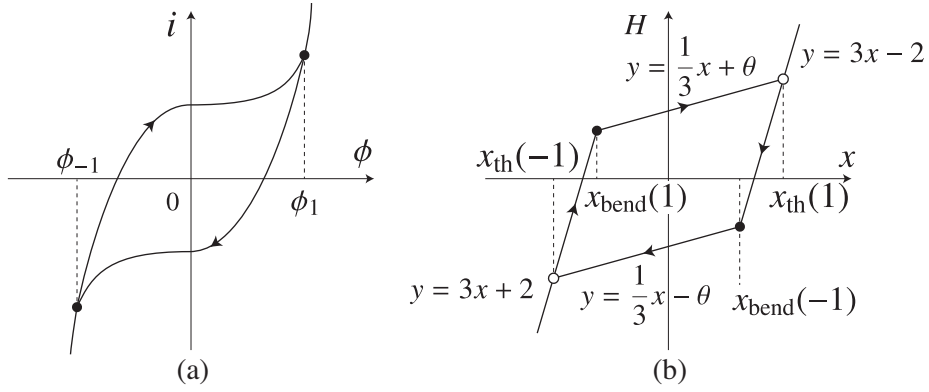


Figure 2: (a) Schematic illustration of the relationship between magnetic flux and current for the saturable-core inductor, and (b) PWL hysteresis H as an approximated model for (a).

the bending point $x_{bend}(\pm 1)$ is added. The thickness of the hysteresis loop of the PWL hysteresis is governed by θ .

2.3. Hybrid systems

We adopt the hybrid system approach[14] to consider a dynamical system containing the PWL hysteresis. Although H is not differentiable at $x_{th}(\pm 1)$ and $x_{bend}(\pm 1)$ and has the hysteresis loop depending on the state, the approach stated below overcomes these difficulties.

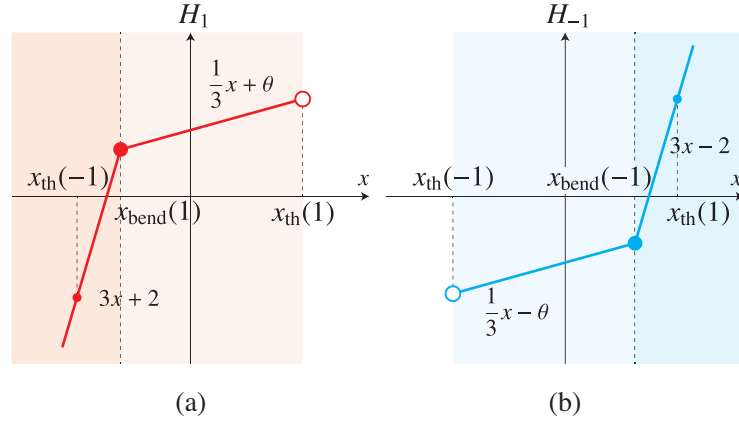


Figure 3: Schematic illustration for divided parts: (a) H_1 and (b) H_{-1} from Fig. 2 (b).

A hybrid system is composed of some smooth dynamical systems and a finite-state machine (FSM). The FSM is a mathematical model used in computation algorithms and this describes the transitions of the finite discrete states (we call *modes*). Each mode gives one dynamical system, and the FSM switches the modes one after another. When we interpret a system as a hybrid system, the total number of the smooth dynamical systems, which is equivalent to the total number of the modes, and the rules of the mode transitions are necessary.

Now we define a hybrid system for the Duffing equation containing the PWL hysteresis. Let m be the total number of the smooth dynamical systems and $M_j \subset \mathbf{R}^2$ and $f_j \subset \mathbf{R}^2$ be the state space under the mode j and the vector field of M_j , respectively. Since one dynamical system has one vector field, m gives how many vector fields we define. For defining f_j , we decompose the PWL hysteresis H into four linear functions. Figure 3 firstly splits H into two parts: H_1 (red shaded) and H_{-1} (blue shaded). H_1 and H_{-1} correspond to upper and lower curves in Fig. 2 (a), respectively. $H_s(x)$ for $s = \pm 1$ is the PWL function of x :

$$H_s(x) = \begin{cases} \frac{1}{3}x + \theta \cdot s & \text{if } |x - x_{\text{th}}(s)| < |x_{\text{th}}(s) - x_{\text{bend}}(s)|, \\ 3x + 2 \cdot s & \text{if } |x - x_{\text{th}}(s)| > |x_{\text{th}}(s) - x_{\text{bend}}(s)|. \end{cases} \quad (4)$$

From Eq. (4), edges $x_{\text{th}}(s)$ and $x_{\text{bend}}(s)$ are given as functions of s with the parameter θ : $x_{\text{th}}(s) = 3(\theta + 2)s/8$ and $x_{\text{bend}}(s) = 3(\theta - 2)s/8$. $H_{\pm 1}(x)$ is defined on two intervals of x edged by $x_{\text{bend}}(\pm 1)$ and $x_{\text{th}}(\pm 1)$:

$$\begin{aligned} I_1 &= \{x \in \mathbf{R} \mid x_{\text{bend}}(1) \leq x \leq x_{\text{th}}(1)\}, \\ I_2 &= \{x \in \mathbf{R} \mid x \leq x_{\text{bend}}(1)\}, \\ I_3 &= \{x \in \mathbf{R} \mid x_{\text{th}}(-1) \leq x \leq x_{\text{bend}}(-1)\}, \\ I_4 &= \{x \in \mathbf{R} \mid x_{\text{bend}}(-1) \leq x\}. \end{aligned} \quad (5)$$

We further decompose $H_s(x)$ into four linear functions g_j of x on I_j :

$$g_1(x) = \frac{1}{3}x + \theta, \quad g_2(x) = 3x + 2, \quad g_3(x) = \frac{1}{3}x - \theta, \quad g_4(x) = 3x - 2.$$

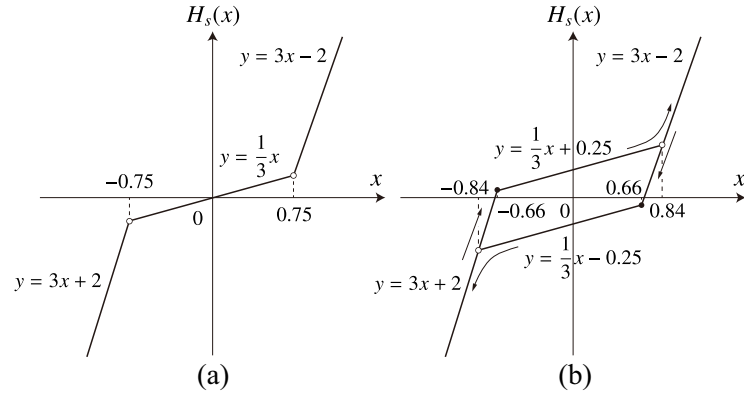


Figure 4: The characteristics of the function $H_s(x)$ with various values of the parameter θ in Eq. (4). (a): $\theta = 0$ and (b): $\theta = 0.25$.

Then M_j is determined by the interval I_j :

$$M_j = \{(x, y) \in \mathbf{R}^2 \mid x \in I_j\}, \quad j = 1 \dots 4, \quad (6)$$

and the vector field f_j in M_j is represented by

$$f_j(t, \mathbf{x}, \lambda) = (y, -ky - g_j(x) + B_0 + B \cos t), \quad (7)$$

where $\mathbf{x} = (x, y) \in \mathbf{R}^2$, λ is a parameter vector. When $\theta = 0$, g_1 and g_2 become the exact same function and H does not include hysteresis anymore, as shown in Fig. 4 (a).

When $\theta \geq 0$, we can derive the following equation:

$$\frac{d\mathbf{x}}{dt} = f_j(t, \mathbf{x}, \lambda), \quad j = 1 \dots 4. \quad (8)$$

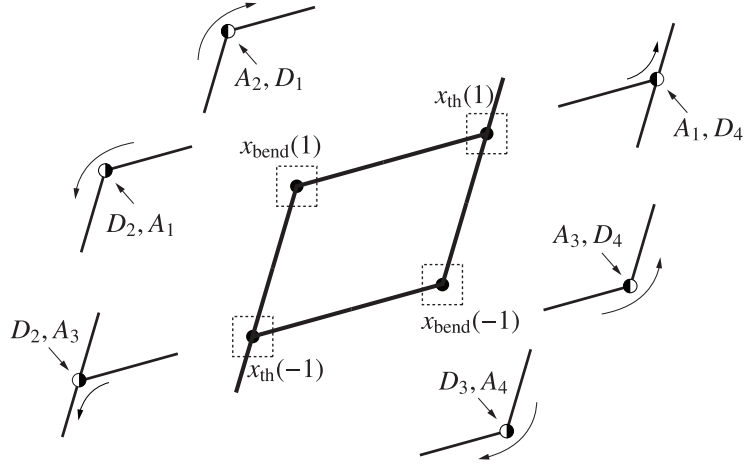


Figure 5: Relationships between arrival and departure sets, and $x = x_{\text{bend}}(\pm 1)$ and $x = x_{\text{th}}(\pm 1)$.

Let D_j and A_j be the departure and arrival sets of mode j :

$$\begin{aligned}
 D_1 &= \{(x, y) \in M_1 \mid x = x_{\text{bend}}(1)\}, \\
 A_1 &= \{(x, y) \in M_1 \mid x = x_{\text{bend}}(1) \text{ or } x = x_{\text{th}}(1)\}, \\
 D_2 &= \{(x, y) \in M_2 \mid x = x_{\text{bend}}(1) \text{ or } x = x_{\text{th}}(-1)\}, \\
 A_2 &= \{(x, y) \in M_2 \mid x = x_{\text{bend}}(1)\}, \\
 D_3 &= \{(x, y) \in M_3 \mid x = x_{\text{bend}}(-1)\}, \\
 A_3 &= \{(x, y) \in M_3 \mid x = x_{\text{th}}(-1) \text{ or } x = x_{\text{bend}}(-1)\}, \\
 D_4 &= \{(x, y) \in M_4 \mid x = x_{\text{bend}}(-1) \text{ or } x = x_{\text{th}}(1)\}, \\
 A_4 &= \{(x, y) \in M_4 \mid x = x_{\text{bend}}(-1)\}.
 \end{aligned} \tag{9}$$

Figure 5 shows the schematic illustration explaining the relationships between D_j and A_j , and $x_{\text{bend}}(\pm 1)$ and $x_{\text{th}}(\pm 1)$. The dynamical system (8) contains the following rules of the mode transitions derived from the features of the saturable-core inductor:

- at $x_{\text{th}}(1)$, a solution in M_1 reaches A_1 , and then the mode is switched from 1 to 4. This process is not invertible.
- at $x_{\text{bend}}(1)$, a solution in M_1 reaches A_1 , and then the mode is switched from 1 to 2. This process is invertible.

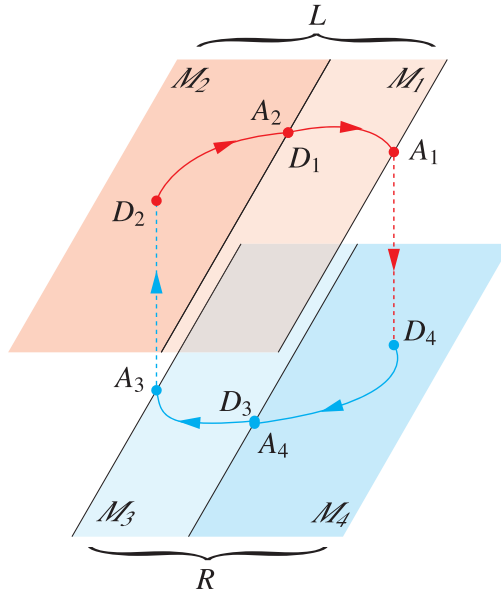


Figure 6: Schematic illustration of the mode transition. Red and blue solid curves are the states of the system.

- at $x_{\text{th}}(-1)$, a solution in M_3 reaches A_3 , and then the mode is switched from 3 to 2. This process is not invertible.
- at $x_{\text{bend}}(-1)$, a solution in M_3 reaches A_3 , and then the mode is switched from 3 to 4. This process is invertible.

Figure 6 helps us understand the above rules. Let $L = M_1 \cup M_2$ and $R = M_3 \cup M_4$ be the closed half-plane. Since the mode transition between the modes 1 and 2 is invertible, the state can freely move in L . For the modes 3 and 4, the same consideration can be made in R . If the state in L goes outside of L , it cannot go back on L with the inverted path because the mode transition between modes 1 and 4 is not invertible. The mode transition between modes 3 and 2 is also similar. In the other words, these transitions between L and R , which are the transitions from mode 1 to mode 4 and from mode 3 to mode 2, are one way only. The FSM representing the rules of the mode transitions for the proposed model is illustrated in Fig. 7.

From the above definitions, the dynamical systems in Eq. (8) and the FSM in Fig. 7 compose a hybrid system with 4 modes. We call this hybrid system the PWL hysteresis

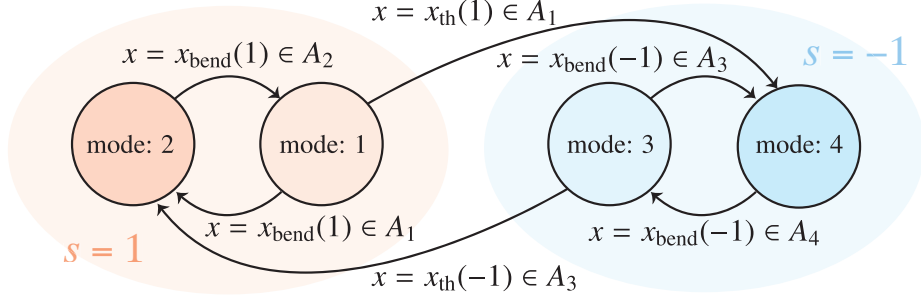


Figure 7: Finite-state machine representing the rules of the mode transitions of the dynamical system (8).

hybrid system.

The solution orbit of this hybrid system with the initial condition $\mathbf{u}_0 = (x_0, y_0)$ is described as a function of the current time t :

$$\mathbf{x}(t) = \boldsymbol{\varphi}(t, \mathbf{x}_0, \boldsymbol{\lambda}) \in \mathbf{R}^2. \quad (10)$$

This solution is actually constructed of some solutions governed by the dynamical system in each mode. Assuming the mode is j after i -times mode transitions, the solution in each mode is given by a function of the current time t , the starting time t_i and the initial value $\mathbf{u}_i = (x_i, y_i) \in D_j$:

$$\begin{aligned} \mathbf{x}_i(t) &= \boldsymbol{\varphi}_i(t, t_i, \mathbf{u}_i, \boldsymbol{\lambda}) \in M_j, \\ \mathbf{x}_i(t_i) &= \boldsymbol{\varphi}_i(t_i, t_i, \mathbf{u}_i, \boldsymbol{\lambda}) = \mathbf{u}_i \in D_j, \quad i = 0, 1, \dots, \end{aligned} \quad (11)$$

where $t_0 = 0$.

3. Method of analysis

In this section, we describe the local stability and bifurcations of periodic solutions of Eq. (8).

A solution orbit is called a periodic solution if it satisfies

$$\mathbf{x}(t + \tau_p) = \mathbf{x}(t), \quad \exists \tau_p \in \mathbf{R}, \forall t \in \mathbf{R}, \quad (12)$$

where $\tau_p > 0$ is the period of the solution. In general, τ_p becomes an integer multiple of 2π , which is the period of f . We achieve numerical integration by using the Runge-Kutta method to compute numerical solutions of the differential and variational equations. We define the step-size of the method as 10^{-2} . Note that the PWL system (8) can be solved analytically in principle because of linearity, however, we rely on numerical computations to avoid treatment about huge numbers of emerged cases.

3.1. Classification of periodic solution

We classify the periodic solution from two standpoints, one is the asymptotic stability (or simply, stability) of it and the other is the mode through which the solution passes.

The stability of a periodic solution is closely related to the stability of the corresponding Poincaré map. We define the Poincaré map T as follows:

$$\begin{aligned} T &: \mathbf{R}^2 \rightarrow \mathbf{R}^2; \\ \mathbf{u}_0 &\mapsto T(\mathbf{u}_0) = \boldsymbol{\varphi}(2\pi, \mathbf{u}_0, \boldsymbol{\lambda}). \end{aligned} \tag{13}$$

In the hybrid system approach, the Poincaré map has another expression as the composition of local maps, which are maps from a departure set to the corresponding arrival set. For simplicity, let $T_i : \Pi_i \rightarrow \Pi_{i+1}$ be a local map and Π_i equal the departure set of (i)-th mode:

$$\begin{aligned} T_0 &: \Pi_0 \rightarrow \Pi_1; \\ &\mathbf{u}_0 \mapsto \mathbf{u}_1 = \boldsymbol{\varphi}_0(t_1, 0, \mathbf{u}_0, \boldsymbol{\lambda}), \\ T_1 &: \Pi_1 \rightarrow \Pi_2; \\ &\mathbf{u}_1 \mapsto \mathbf{u}_2 = \boldsymbol{\varphi}_1(t_2, t_1, \mathbf{u}_1, \boldsymbol{\lambda}), \\ &\vdots \\ T_{n-1} &: \Pi_{n-1} \rightarrow \Pi_0; \\ &\mathbf{u}_{n-1} \mapsto \mathbf{u}_n = \boldsymbol{\varphi}_{n-1}(2\pi, t_{n-1}, \mathbf{u}_{n-1}, \boldsymbol{\lambda}), \end{aligned} \tag{14}$$

where n is the total number of the mode transitions. Note that Π_i also equals the arrival set of ($i - 1$)-th mode if $i \neq 0$. The Poincaré map as a composition of local maps forms

$$T(\mathbf{u}_0) = T_{n-1} \circ T_{n-2} \circ \cdots \circ T_0(\mathbf{u}_0). \tag{15}$$

Table 1: Symbols for the classification of an l -periodic point by its local stability.

Symbol	Stability	Condition
${}_0D^l$	completely stable	$ \mu_1 < 1, \mu_2 < 1$
${}_1D^l$	directly unstable	$0 < \mu_1 < 1, 1 < \mu_2$
${}_1I^l$	inversely unstable	$\mu_1 < -1, -1 < \mu_2 < 0$
${}_2D^l$	completely unstable	$ \mu_1 > 1, \mu_2 > 1$

When the \mathbf{u}_0 satisfies

$$\mathbf{u}_0 = T(\mathbf{u}_0), \quad (16)$$

then \mathbf{u}_0 is called a fixed point of the Poincaré map. The point that satisfies

$$\mathbf{u}_0 = T^l(\mathbf{u}_0), \quad l = 1, 2, \dots \quad (17)$$

is called an l -periodic point of the Poincaré map. In this sense, the fixed point equals to the 1-periodic point. Thus, the fixed points and l -periodic points are collectively called periodic points in this study. The problems to obtain solutions for Eq. (16) or (17) are equivalent to the boundary value problems. We use Newton's method to calculate their solutions. The Jacobian matrix $DT(\mathbf{u}_0)$ of the Poincaré map $T(\mathbf{u}_0)$ is necessary to use Newton's method. Since T is the composition of the local maps as shown in Eq. (15), a special method to calculate DT is needed. For a detailed explanation of the method, refer to our previous study[15].

The Jacobian matrix $DT^l(\mathbf{u}_0)$ gives the stability of l -periodic points \mathbf{u}_0 as the characteristic multiplier μ derived from the characteristic equation of $DT^l(\mathbf{u}_0)$:

$$\chi(\mu) = \det(DT^l(\mathbf{u}_0) - \mu I) = 0, \quad (18)$$

where I is a 2×2 identity matrix. Since this system is 2-dimensional, two characteristic multipliers μ_1 and μ_2 are obtained. Table 1 shows the classification of an l -periodic point by its stability. From Liouville's formula, it is noteworthy that ${}_2D^l$ does not exist in the Duffing equation when $k > 0$. We regard $k > 0$ in this study.

On the other hand, for the hybrid systems, we should classify periodic points by the modes through which the corresponding solutions pass. In this study, the periodic

Table 2: Symbols for the classification of a periodic point by the modes through which the corresponding solution passes.

Symbol	Type
[L]	a left type
[R]	a right type
[(LR) ^p]	a <i>p</i> -loops left-right type

solution passing through only the half-plane *L* is called left type periodic solution. Likewise, the periodic solution passing through only the half-plane *R* is called right type periodic solution. If a periodic solution passes through both the half-planes, it passes through each plane in the same number of times within the period of the solution. Given *p* is this number of times, let us call such solutions the *p*-loops left-right type periodic solution. The periodic points included in each type periodic solution are also called with its type: left, right, or *p*-loops left-right type periodic points, respectively. Table 2 shows the symbols that are additionally attached to the symbols shown in Tab. 1 to classify periodic points by the modes.

3.2. Local bifurcations

Let us consider an *l*-periodic point with an arbitrary value of the parameter λ . As varying λ until λ^* where the absolute value of μ becomes 1, the local bifurcation of the *l*-periodic point occurs. Since the appearance scenario of the local bifurcation is independent of the modes, each type of the *l*-periodic point classified by the modes can meet the local bifurcation.

In the case that $\mu = 1$, equivalently $\chi(1) = 0$, a tangent bifurcation occurs. This bifurcation generates a couple of stable and unstable *l*-periodic points. These topological changes are expressed by the following:

$$\begin{aligned}
 \emptyset &\Leftrightarrow {}_0D^l[L] + {}_1D^l[L], \\
 \emptyset &\Leftrightarrow {}_0D^l[R] + {}_1D^l[R], \\
 \emptyset &\Leftrightarrow {}_0D^l[(LR)^p] + {}_1D^l[(LR)^p],
 \end{aligned} \tag{19}$$

where the symbol \Leftrightarrow indicates the relation before and after the bifurcation and \emptyset means there are no periodic points. In the case that $\mu = -1$, equivalently $\chi(-1) = 0$, a period-

doubling bifurcation occurs. This bifurcation changes the stability of an l -periodic point and generates two $2l$ -periodic stable points. In this instance, the bifurcation is called period-doubling bifurcation of an l -periodic point. These topological changes are expressed by the following:

$$\begin{aligned}
{}_0D^l[L] &\Leftrightarrow {}_1I^l[L] + 2 {}_0D^{2l}[L], \\
{}_0D^l[R] &\Leftrightarrow {}_1I^l[R] + 2 {}_0D^{2l}[R], \\
{}_0D^l[(LR)^p] &\Leftrightarrow {}_1I^l[(LR)^p] + 2 {}_0D^{2l}[(LR)^p], \\
{}_1I^l[L] &\Leftrightarrow {}_0D^l[L] + 2 {}_1D^{2l}[L], \\
{}_1I^l[R] &\Leftrightarrow {}_0D^l[R] + 2 {}_1D^{2l}[R], \\
{}_1I^l[(LR)^p] &\Leftrightarrow {}_0D^l[(LR)^p] + 2 {}_1D^{2l}[(LR)^p].
\end{aligned} \tag{20}$$

Note that there are no Neimark-Sacker bifurcations since there is no ${}_2D^l$ with $k > 0$. The parameter set where a bifurcation arises is called a bifurcation set. In this study, G^l and I^l are symbols denoting the tangent and period-doubling bifurcation sets of an l -periodic point, respectively.

We can obtain a tangent bifurcation set in a hybrid system by simultaneously solving Eq. (17) and $\chi(1) = 0$ with Newton's method[2]. A period-doubling bifurcation set is also similar. We compute the 2-parameter bifurcation diagram of the local bifurcations by using parameter continuation.

3.3. Grazing bifurcation

If a continuous time dynamical system includes the mode transitions depending on the state, a grazing bifurcation arises[16]. This bifurcation is observed if the solution grazes a boundary that changes the mode of a system.

Conditions of raising a grazing bifurcation are given as follows:

$$\begin{cases} q_s(\mathbf{x}(\tau_{th})) = 0, \\ \frac{dq_s}{dt} = 0, \end{cases} \tag{21}$$

where $q_s : \mathbf{R}^2 \rightarrow \mathbf{R}$ is the function of \mathbf{x} and is governed by the location of the boundary,

τ_{th} is the time when the solution grazes the boundary, and

$$\frac{dq_s}{dt} = \frac{\partial q_s}{\partial \mathbf{x}} \frac{d\boldsymbol{\varphi}}{dt} \Big|_{t=\tau_{\text{th}}}. \quad (22)$$

In this study, $q_s(\mathbf{x}) = x - x_{\text{th}}(s)$. As varying some parameter, the periodic solution can graze the boundary, and then the mode of the system changes. At that time, the periodic solution cannot keep its structure anymore. Hence, grazing bifurcation extinguishes periodic points:

$$\begin{aligned} \emptyset &\Leftrightarrow {}_0D^l[L], \\ \emptyset &\Leftrightarrow {}_0D^l[R], \\ \emptyset &\Leftrightarrow {}_0D^l[(LR)^p], \\ \emptyset &\Leftrightarrow {}_1D^l[L], \\ \emptyset &\Leftrightarrow {}_1D^l[R], \\ \emptyset &\Leftrightarrow {}_1D^l[(LR)^p], \\ \emptyset &\Leftrightarrow {}_1I^l[L], \\ \emptyset &\Leftrightarrow {}_1I^l[R], \\ \emptyset &\Leftrightarrow {}_1I^l[(LR)^p]. \end{aligned} \quad (23)$$

In this study, Z^l is the symbol denoting the grazing bifurcation set of an l -periodic point. Grazing bifurcations can arise for both stable and unstable solutions.

Grazing bifurcation sets are obtained by solving boundary value problem Eq. (21). Therefore, the bifurcation sets are calculated by using Newton's method.

3.4. Typical bifurcation structure

Let us introduce the typical bifurcation scenario of a 2-periodic point existing in the PWL hysteresis hybrid system. Assume that the corresponding periodic solution passes through both modes one-time-only within its period as shown in Fig. 8 (b). At the vertical line labeled G^2 in Fig. 8 (a), tangent bifurcation arises and two periodic points are generated in accordance with the third equation of Eq. (19): a stable one ${}_0D^2[(LR)^1]$ and an unstable one ${}_1D^2[(LR)^1]$ as shown in Fig. 8 (b). Note that they are too close and difficult to be confirmed by our eyes. As B increases, these points move further apart. Afterward, at $B = 0.339$, ${}_1D^2[(LR)^1]$ reaches Z^2 , where the corresponding

solution orbit is shown in Fig. 8 (c), and suddenly disappears in accordance with the sixth equation in Eq. (23). Similarly, ${}_0D^2[(LR)^1]$, whose solution orbit is shown in Fig. 8 (d), also reaches Z^2 at $B = 0.356$ and disappears in accordance with the third equation in Eq. (23).

4. Results of analysis

In this section, we explore the phase space $x \in (-2, 2) \subset \mathbf{R}$ and $y \in (-2, 2) \subset \mathbf{R}$ with the parameter space $B \in (0, 0.7) \subset \mathbf{R}$ and $B_0 \in (0, 0.7) \subset \mathbf{R}$.

4.1. Bifurcation diagrams and response curves

In this subsection, we deal with the Duffing equation and two types of the hybrid systems with various $H_s(x)$ shown in Fig. 4. When $\theta = 0$, the hybrid system does not include the hysteresis in itself, and then it is called the PWL hybrid system. We set the parameter $k = 0.2$.

By applying the method mentioned in Sec. 2 to the systems, 2-parameter bifurcation diagrams and response curves of them are obtained as shown in Fig. 9. Figure 9 (a) shows a 2-parameter bifurcation diagram of the Duffing equation. Note that the results have already been stated by Kawakami[2] and are restated here for comparison with the result of the analysis for the PWL ones.

In Fig. 9 (a), there is a period-doubling bifurcation set I^1 with the shape of a closed curve in the lower region of B_0 ; however, in Fig. 9 (b), the corresponding bifurcation sets are not located. This is because the corresponding solutions of the PWL hybrid system are confined in the domain M_1 (or equivalently M_3), i.e., the system does not have nonlinearity. On the other hand, the upper region in Fig. 9 (b) contains the positive slopes of I^1 and G^1 that are not observed in the Duffing equation. They are caused by the nonlinearity around the bending boundary $x_{\text{bend}}(-1)$. The solution with some parameter does not pass through $x_{\text{bend}}(s)$. We can easily calculate such solutions without any numerical method because they are the solutions of a linear ordinary differential equation. Moreover, we can calculate the parameter space where

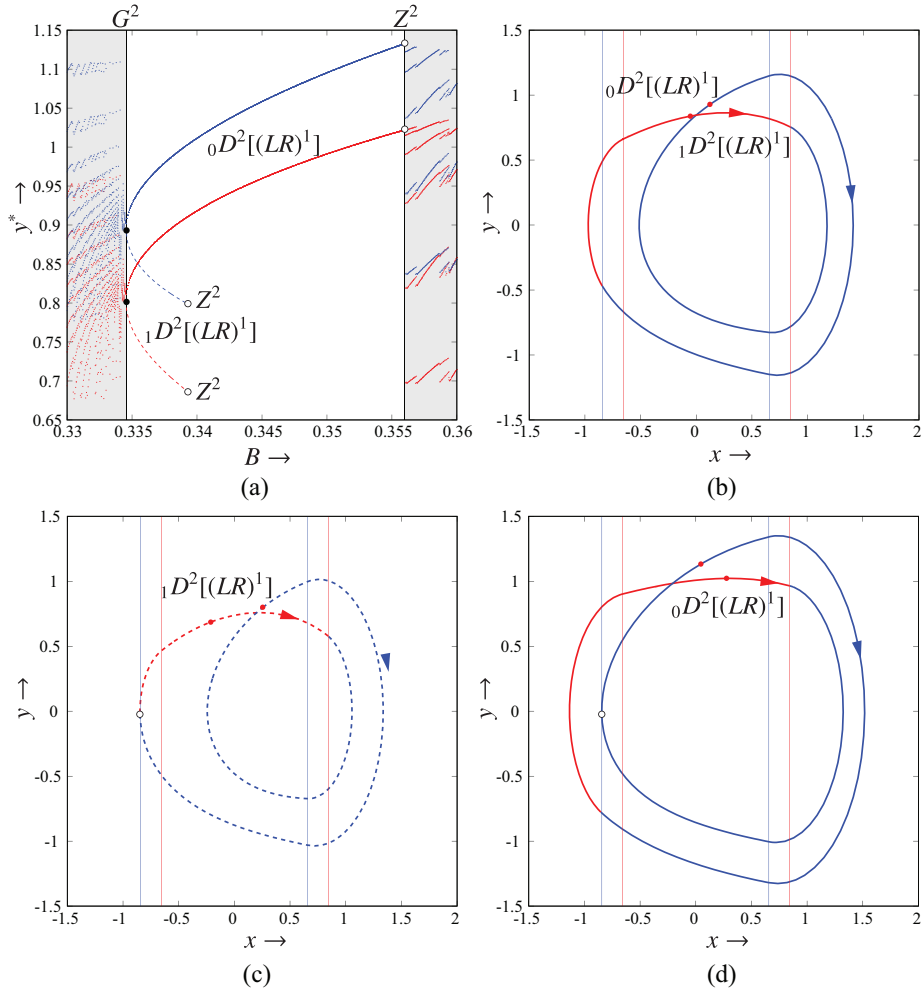


Figure 8: (a) 1-parameter bifurcation diagram of the PWL hysteresis hybrid system with $\theta = 0.25$, $k = 0.2$, $B_0 = 0.2$ and $B \in (0.33, 0.36)$. In the central region, solid and broken curves are stable and unstable periodic points, respectively. Tangent bifurcation arises at the parameter with black dots and the grazing bifurcations arise at the parameter with open circles. (b) Phase portrait with $B = 0.335$ corresponding G^2 . (c) Phase portrait with $B = 0.339$ corresponding Z^2 of ${}_1D^2[(LR)^1]$. (d) Phase portrait with $B = 0.356$ corresponding Z^2 of ${}_0D^2[(LR)^1]$. In (b), (c) and (d), vertical lines are $x_{th}(\pm 1)$ and $x_{bend}(\pm 1)$ where the mode transitions arise.

such solution exists. Focusing on ${}_0D^1[R]$ with $\theta = 0$, the parameter region is given by

$$B_0 > 1.493B + 0.25. \quad (24)$$

The edge of this parameter space is along the positive slope of I^1 and G^1 in Fig. 9 (b). If parameters are outside of this space, the solution with the parameters comes to pass through $x_{\text{bend}}(-1)$, i.e., this solution comes to include nonlinearity in itself. Afterward, tangent and period-doubling bifurcations arise at G^1 and I^1 . Next, the bifurcation set labeled as $Z^1 + Z^1$ in Fig. 9 (b) is the parameter set where different two grazing bifurcation arises at the same time. They are the bifurcations from completely different solutions, see at P_4 in Fig. 9 (b). They are with the same region coincidentally and, as an interesting result, correspond to G^1 at P_2 in Fig. 9 (d). The set $Z_1 + Z_1$ goes across the parameter plane from the lower part of B_0 to the upper. When they join the curve G^1 at the outlined circle near $(B, B_0) = (0.25, 0.4)$, Z^1 of ${}_1D^1[R]$ becomes Z^1 of ${}_0D^1[R]$. In other words, the stability of the periodic point reaching Z^1 changes.

Comparing with Fig. 9 (b), the positive slopes of I^1 and G^1 in Fig. 9 (c) are located in the lower region of parameter space. Similarly to Eq.(24), we can calculate the line including the bending boundary $x_{\text{bend}}(-1)$:

$$B_0 > 1.493B - 0.031. \quad (25)$$

The edge $B_0 = 1.493B - 0.031$ is at the lower side of the edge $B_0 = 1.493B + 0.25$. Similarly to that the bifurcation sets in Fig. 9 (b) are along this edge, they in Fig. 9 (c) also go down along the edge. On the other hand, $Z^1 + Z^1$ are separated into two parameter sets: Z^1 including P_6 and Z^1 including P_9 , because of the hysteresis. If the system does not include hysteresis, solutions freely come and go through the border $x_{\text{th}}(s)$. However, if the system includes hysteresis, solutions can go across the border from the left/right part but cannot come back from the opposite part. Because of this difference, complex and confusing phenomena arise after the grazing bifurcation at Z^1 including P_6 , as shown in Fig. 9 (f). With the parameters in the upper part of the shaded region in the figure, the solutions have a much higher number of p . We can also

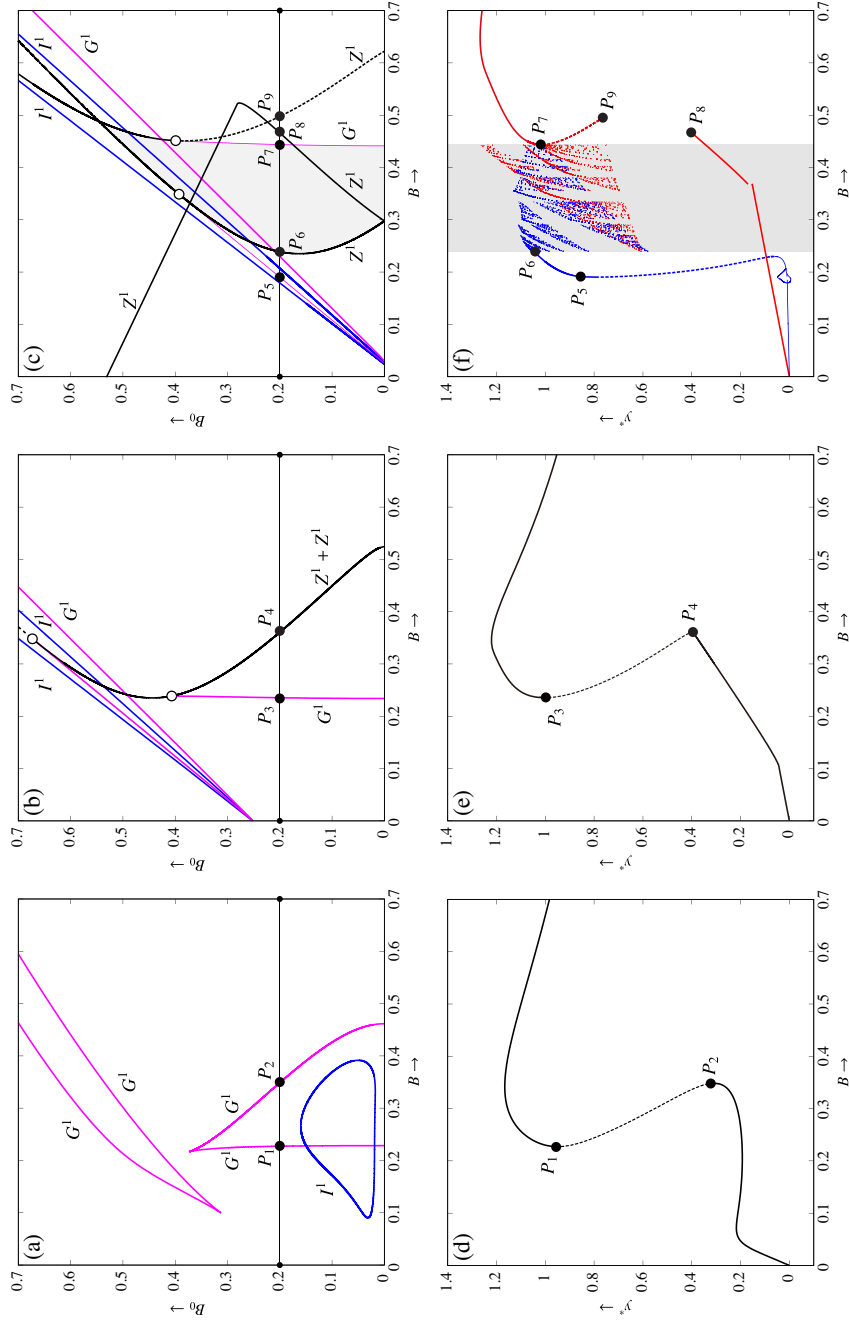


Figure 9: Upper row: 2-parameter (B - B_0) bifurcation diagrams with $0 < B < 0.7$, $0 < B_0 < 0.7$. Lower row: diagrams of the response curves of y^* with $0 < B < 0.7$, $B_0 = 0.2$, where y^* is the coordinate value of y of the Poincaré map. (a) and (d): the Duffing equation. (b) and (e): the PWL hybrid system ($\theta = 0.0$). Fig. 4 (a)), (c) and (f): the PWL hysteresis hybrid system ($\theta = 0.25$, Fig. 4 (b)). In (d) – (f), solid curves present stable periodic solutions and broken curves present unstable periodic solutions. P_i s are the point with common parameter sets between a bifurcation diagram and a diagram of response curves.

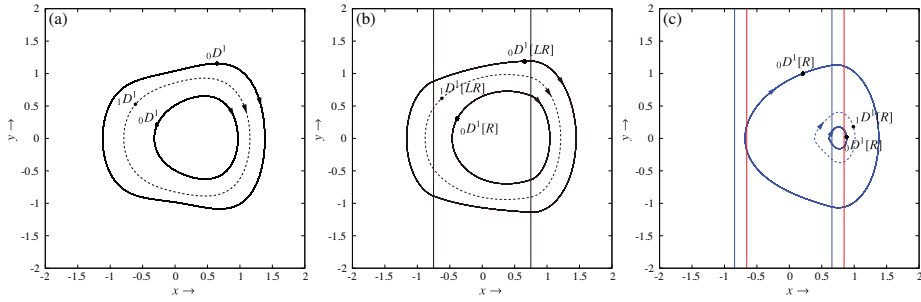


Figure 10: Phase portraits of the resonant and non-resonant solutions in (a): the Duffing equation with $(B, B_0) = (0.3, 0.2)$, (b): the PWL hybrid system with $\theta = 0.0$ and $(B, B_0) = (0.3, 0.2)$, and (c): the PWL hysteresis hybrid system with $\theta = 0.25$ and $(B, B_0) = (0.3, 0.2)$. Vertical lines in (b) are the sets of $x_{th}(s)$ and x_{bend} , and they in (c) are the sets of $x_{th}(s)$ and x_{bend} . Solid and broken curves represent stable and unstable periodic solutions, respectively.

observe such phenomena in the shaded region enclosed by the Z^1 in Fig. 9 (c). In the next section, we discuss these phenomena in detail. Z^1 in Fig. 9 (c) with a negative slope starting from $(B, B_0) = (0, 0.53)$ is a newly observed grazing bifurcation set of the periodic point $0D^1[L]$ whose orbit exists only in the domain M_1 . The movement of $0D^1[L]$ as parameter varying is shown as a red line in Fig. 9 (f).

In Fig. 9 (d) and 9 (e), we can confirm nonlinear resonance phenomena arising around $B = 0.3$. When this phenomenon arises, there exist the parameter sets representing two different solutions of the system. Considering the solutions with such parameters, we call the solution with larger amplitude a resonant solution and call the smaller one a non-resonant solution. The same phenomenon is observed around $B = 0.2$ in Fig. 9 (f). Figure 10 shows phase portraits of the co-existing solutions introduced above.

4.2. Devil's staircase

The shaded region in Fig. 9 (c) and (f) contains many tangent and grazing bifurcation sets of stable and unstable periodic points. 1-parameter bifurcation diagram is a useful tool to confirm the appearance of the bifurcations of stable periodic points. To obtain the diagram, we compute images of a point under 10,000 iterations of the Poincaré maps and use the last 1,000 points for the data to plot. Figure 11 shows the result of the computing and also shows the movement of the ratio ρ , which is given later, and the

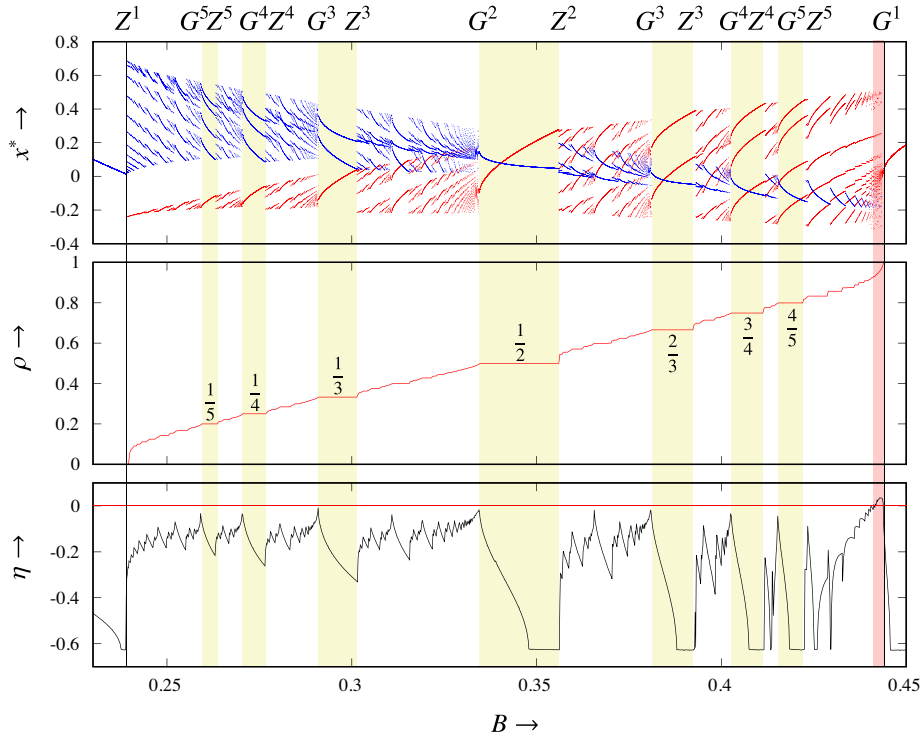


Figure 11: 1-parameter bifurcation diagram of x^* , with the ratio ρ and the maximal Lyapunov exponent η with $B \in (0.23, 0.45)$. $B_0 = 0.2$. x^* is the coordinate value of x of the Poincaré map.

maximal Lyapunov exponent.

In the 1-parameter bifurcation diagram in Fig. 11, as B increases, the period of the Poincaré map keeps changing because of raising tangent and grazing bifurcations. Let us confirm this changing with the phase portraits of the corresponding solutions. Figure 12 shows the solutions with $B \in (0.23, 0.45)$ and $B_0 = 0.2$. As B increases from $B = 0.239$, the periodic solution shown in Fig. 12 (a) reaches $x_{th}(1)$ and gets grazing bifurcation Z^1 , i.e., the solution immediately disappears. Afterward, another periodic solution shown in Fig. 12 (b) appears. Likewise, as B increases from here, disappearance and appearance arise one after another with $B \in (0.23, 0.45)$. With some parameters in such parameter space, a solution becomes to have quite long periods, as shown in Fig. 12 (f). As B increases further, tangent bifurcation for a 2-periodic point ${}_0D^2[(LR)^1]$ arises, as shown at the parameter labeled with G^2 in Fig. 12 (g). For a

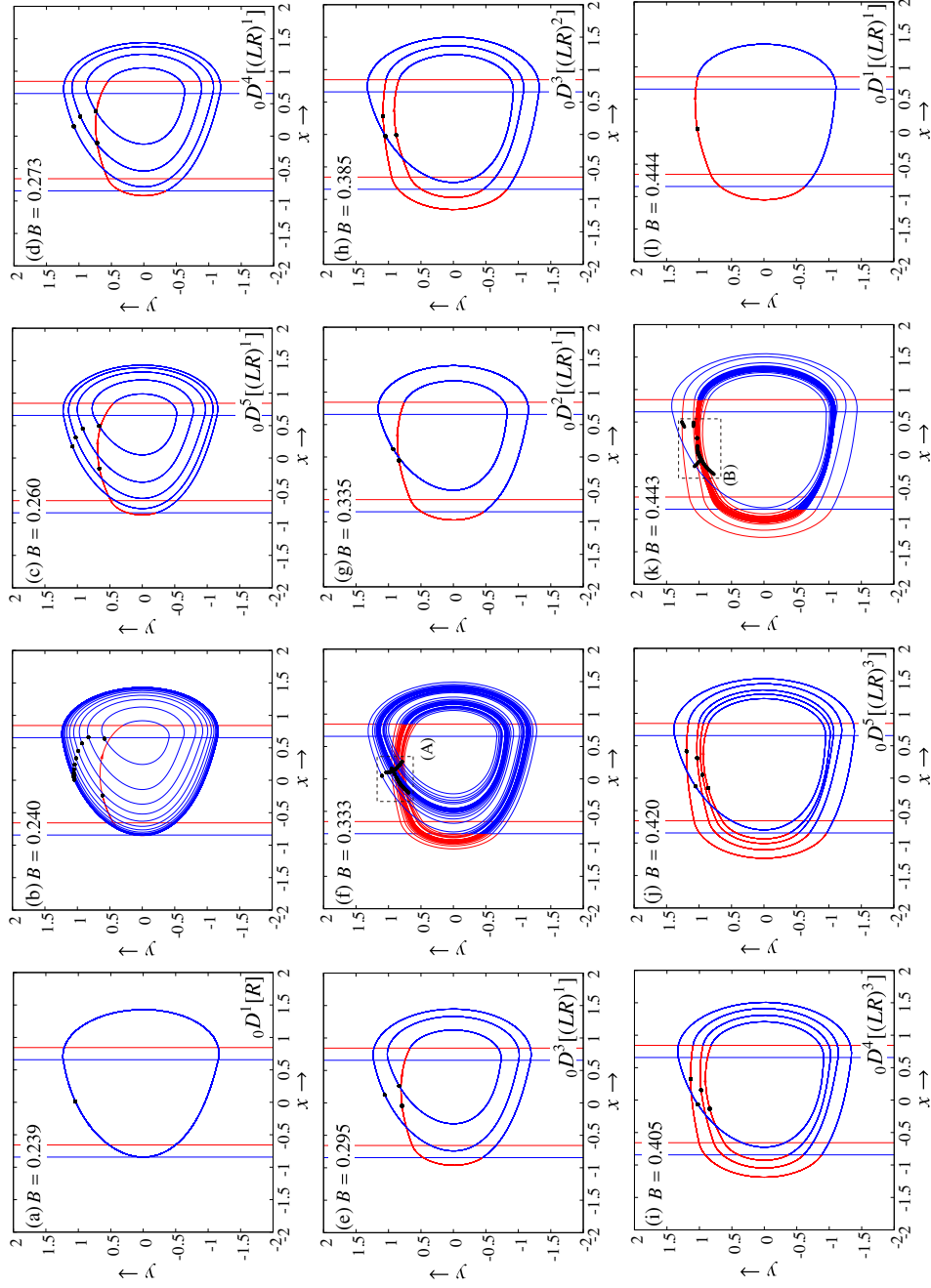


Figure 12: Phase portraits of the PWL hysteresis hybrid system with $\theta = 0.25$ and $B_0 = 0.2$.

concrete discussion, refer to Fig. 8, which shows an example of this tangent bifurcation and the subsequent grazing bifurcation. The 2-periodic point ${}_0D^2[(LR)^1]$ arises with an unstable 2-periodic point ${}_1D^2[(LR)^1]$ because of the feature of tangent bifurcation in Eq. (19). ${}_1D^2[(LR)^1]$ disappears very soon with raising grazing bifurcation. This grazing bifurcation is invisible in responses because this is a bifurcation for an unstable periodic point, After this bifurcation, ${}_0D^2[(LR)^1]$ disappears because of the different grazing bifurcation. From here, the sequence of tangent and grazing bifurcations continues until at $B = 0.44$. Finally, the solution stabilizes as a 1-periodic solution through ${}_0D^1[(LR)^1]$, as shown in Fig. 12 (l). On the other hand, chaos is observed with $B = 0.443$, as shown in Fig. 12 (k). Figure 13 (a) and (b) show the enlargements of the regions (A) and (B) in Fig. 12 (f) and (k) that focus on the Poincaré map of each solution. Figure 13 (c) and (d) show the return map of the solutions.

Given p_k is the number of times that a solution passes through both the half-planes from $t = 0$ to $t = 2k\pi$, the ratio ρ indicates the average value of this number within the time of 2π :

$$\rho = \lim_{k \rightarrow \infty} \frac{p_k}{k}. \quad (26)$$

For example, ρ of the solution shown in Fig. 12 (g) is almost $1/2$ because the orbit passes through both the half-planes at once within two iterations of Poincaré maps. The middle part of Fig. 11 depicts the movement of the ratio ρ as B varies. As B increases, we find that ρ grows as well as the shape of the devil's staircase. At this instance, ρ changes its value by undergoing tangent and grazing bifurcations. This results in that the devil's staircase shown in this model is caused by the tangent bifurcations and the grazing bifurcations. As a characteristic behavior of the devil's staircase, ρ grows in accordance with Farey sequence. For example, between $\rho = 1/2$ and $\rho = 2/3$, there are parameters where $\rho = (1 + 2)/(2 + 3) = 3/5$. Additionally, the devil's staircase of unstable periodic solutions might also arise although we could not observe it naturally. This consideration is based on the fact that there are grazing bifurcations for the unstable periodic solutions as well as the stable periodic solutions. The devil's staircase is a phenomenon ordinary observed in discrete time dynamical systems. Therefore, it is very interesting to find this phenomenon in a hybrid system. As a further interesting

fact, the phenomenon we observed is caused by the result of the sequence of tangent and grazing bifurcations. In other words, in the hybrid systems, the sequence of tangent and grazing bifurcations fractally generates and erases periodic solutions one after another and forms the devil's staircase.

The maximal Lyapunov exponent:

$$\eta = \lim_{k \rightarrow \infty} \frac{1}{k} \log \frac{\|DT^k(\mathbf{u}_0)\mathbf{e}\|}{\|\mathbf{e}\|}, \quad (27)$$

where \mathbf{e} is an arbitrary unit vector, indicates whether the attractor is chaotic or not. The bottom part of Fig. 11 presents the movement of the maximal Lyapunov exponent η with varying B . Since η is positive at $B = 0.443$, the solution shown in Fig. 12 (k) is recognized as chaos. With $k = 0.1$, the parameter space where the solution becomes chaotic gets larger than the case of $k = 0.2$, as shown as the red shaded region in Fig. 14. As an interesting phenomenon, we found that the crisis C arises around $B = 0.145$ with $k = 0.1$. A crisis is the appearance (or disappearance) of the chaotic attractor as the parameters of a system are varied[17].

It is important to confirm robustness and reproducibility of phenomena shown in this paper, hence we note here a brief analysis of noise margin. If we scan the one-dimensional bifurcation diagram with the presence of the thermal noise as an additive Gaussian noise, then the system retains almost the same bifurcation structure collated with Fig. 11, i.e., the system exhibits the devil's staircase even though the noise has a comparatively large amplitude. This result implies the PWL hysteresis hybrid system is structurally stable with the defined parameters.

All mentioned results in this section are not observed in the Duffing equation or the PWL hybrid system; therefore, we consider that they are unique results observed in the PWL hysteresis hybrid system.

5. Conclusion

We studied the phenomena observed in a forced planer system with a piecewise linear hysteresis. We modeled the dynamics as a hybrid system, that is, the pair of a finite-state machine (FSM) and continuous time dynamical systems. The periodic

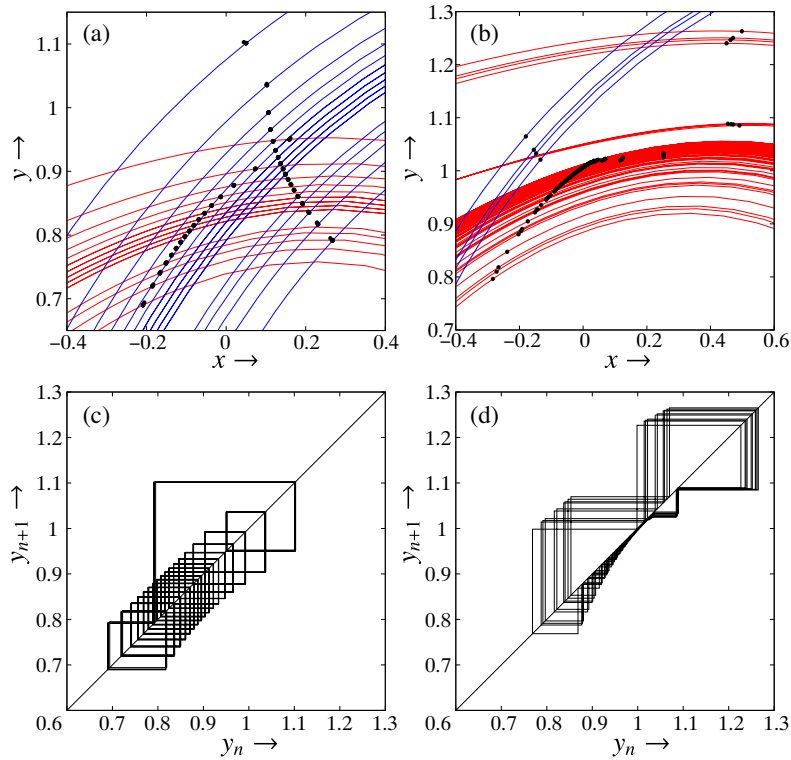


Figure 13: (a), (b) Enlargements of regions (A) and (B) in Fig. 12 (f) and (k). (c), (d) Return maps of y of the solution with the parameters in Fig. 12 (f) and (k).

solutions are interpreted as the periodic points of the Poincaré map, and all possible periodic points are classified with the topological indices, which represent the stability of the periodic points and the modes through which the solution passes. The main results are summarized below:

- The local bifurcation sets such as tangent and period-doubling bifurcation sets observed in the hybrid systems are computed and presented as 2-parameter bifurcation diagrams, see Fig. 9.
- Grazing bifurcations arise; and they are also traced, as shown in Fig. 9. This bifurcation is a representative phenomenon of the switched dynamical systems.
- A nonlinear resonance, which is a typical phenomenon in the Duffing equation, is also found to arise in the PWL hysteresis one, see Fig. 10.

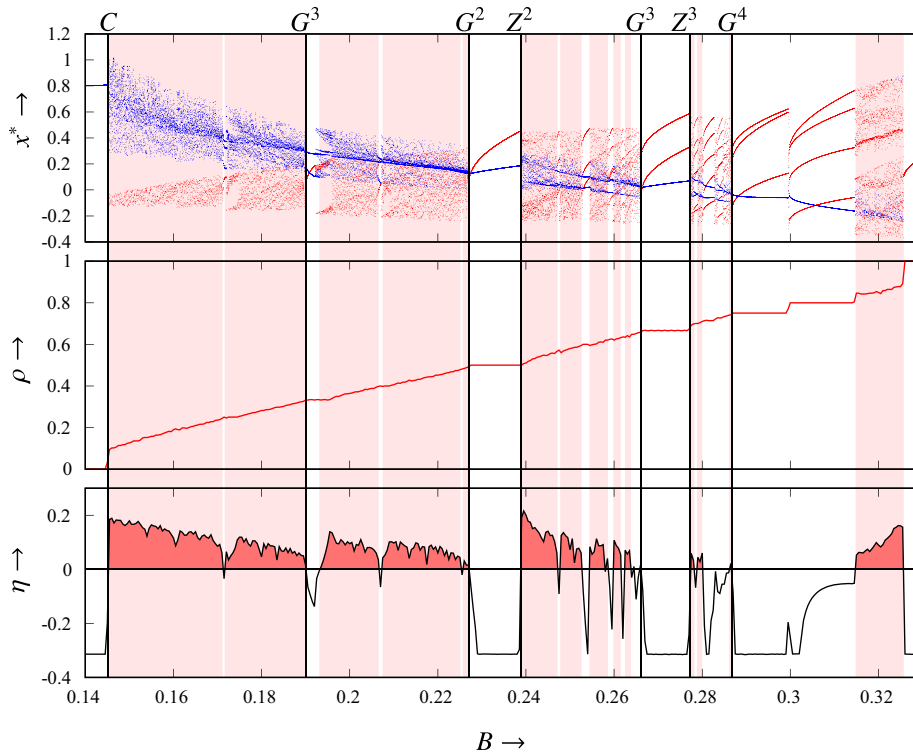


Figure 14: 1-parameter bifurcation diagram of x^* , the ratio ρ and η with $k = 0.1$, $B \in (0.14, 0.33)$ and $B_0 = 0.2$. Chaos arises in red shaded regions.

- The sequence of tangent and grazing bifurcations caused by the effect of the hysteresis is found in the 1-parameter bifurcation diagram. This phenomenon causes the devil's staircase in the value of the ratio ρ and is a representative phenomenon of this system, see Fig. 11 and 14.
- When the damping coefficient k becomes small as $k = 0.1$, many chaotic solutions are observed, and the parameter space where we can observe them is located in the 1-parameter bifurcation diagrams with their the maximal Lyapunov exponent of the solution, see Fig. 14.

The most remarkable result of this paper is the discovery of the devil's staircase in a hybrid system. As a future work, we are interested in the correspondence between the devil's staircase of the PWL hysteresis hybrid system and discrete time dynamical systems. Additionally, we should consider the global bifurcation problem.

References

- [1] C. Hayashi, Y. Ueda, H. Kawakami, Transformation theory as applied to the solutions of non-linear differential equations of the second order, *Int. J. Non. Linear. Mech.* 4 (3) (1969) 235–255.
- [2] H. Kawakami, Bifurcation of periodic responses in forced dynamic nonlinear circuits: Computation of bifurcation values of the system parameters, *IEEE Trans. Circuits Syst.* 31 (3) (1984) 248–260.
- [3] I. Kovacic, M. J. Brennan, *The Duffing equation: nonlinear oscillators and their behaviour*, John Wiley & Sons, 2011.
- [4] H. Nijmeijer, H. Berghuis, On Lyapunov control of the Duffing equation, *IEEE Trans. Circuits Syst. I* 42 (8) (1995) 473–477.
- [5] C. Hayashi, *Nonlinear Oscillations in Physical Systems*, McGraw Hill, 1964.
- [6] C. Hayashi, The influence of hysteresis on nonlinear resonance, *Journal of the Franklin Institute* 281 (5) (1966) 379 – 386.
- [7] T. Saito, An approach toward higher dimensional hysteresis chaos generators, *IEEE Trans. Circuits Syst.* 37 (3) (1990) 399–409.
- [8] Y. Nishio, S. Mori, Chaotic phenomena in an LCR oscillator with a hysteresis inductor, in: *Proc. ISCAS, IEEE*, 2873–2876, 1991.
- [9] K. Kimura, S. Suzuki, T. Tsubone, T. Saito, The cylinder manifold piecewise linear system: Analysis and implementation, *Nonlinear Theory and Its Applications, IEICE* 6 (4) (2015) 488–498.
- [10] T. Kousaka, T. Ueta, H. Kawakami, Bifurcation of switched nonlinear dynamical systems, *IEEE Trans. Circuits Syst.* 46 (7) (1999) 878–885.
- [11] M. Bernardo, F. Garefalo, L. Glielmo, F. Vasca, Switchings, bifurcations, and chaos in DC/DC converters, *IEEE Trans. Circuits Syst. I: Fundamental Theory and Applications* 45 (2) (1998) 133–141.

- [12] E. M. Izhikevich, Simple model of spiking neurons, *IEEE Trans. Neural Networks* 14 (6) (2003) 1569–1572.
- [13] Y. Ma, M. Agarwal, S. Banerjee, Border collision bifurcations in a soft impact system, *Physics Letters A* 354 (4) (2006) 281–287.
- [14] E. A. Lee, S. A. Seshia, *Introduction to embedded systems: A cyber-physical systems approach*, Lee & Seshia, 2011.
- [15] Y. Miino, D. Ito, T. Ueta, A computation method for non-autonomous systems with discontinuous characteristics, *Chaos, Solitons & Fractals* 77 (2015) 277–285.
- [16] M. Bernardo, A. R. Champneys, C. J. Budd, P. Kowalczyk, *Qualitative theory of non-smooth dynamical systems*, Springer London, London, 47–119, 2008.
- [17] C. Grebogi, E. Ott, J. A. Yorke, Crises, sudden changes in chaotic attractors, and transient chaos, *Physica D: Nonlinear Phenomena* 7 (1-3) (1983) 181–200.